

# The effect of additives on the hydration of $\text{CaSO}_4 \cdot 0.5\text{H}_2\text{O}$ : A synchrotron X-ray diffraction study

Sebastian J. Gurgul <sup>a</sup>, Gabriel Seng <sup>b</sup> and Gareth R. Williams <sup>a\*</sup>

<sup>a</sup> UCL School of Pharmacy, University College London, 29-39 Brunswick Square, London, WC1N 1AX, UK

<sup>b</sup> Etex Group, 500 Rue Marcel Demonque, Avignon, 84000, France

## Abstract

To modulate the rate of hydration of calcium sulfate hemihydrate (HH) to calcium sulfate dihydrate for industrial applications, additives (both accelerants and retardants) are added to the HH. Here we explore in detail the kinetics and mechanism of HH hydration in the presence of the accelerators  $\text{K}_2\text{SO}_4$  or  $\text{ZnSO}_4$ , and also when a retardant (citric acid or tartaric acid) is added. Retardants tend to lower the maximum temperature of the reaction and increase the time needed to reach 50% hydration, yet the total conversion percentage is much higher for citric acid/tartaric acid than when an accelerant is added. The reaction process is found to involve heterogenous nucleation regardless of the nature of the additive. More soluble accelerants act mainly through increasing the rate of crystal growth, while less soluble species have a more significant effect on the rate of nucleation.

Keywords: kinetics, gypsum, plasterboards, additives, hydration

## Abbreviations:

<b>BMA</b>	Ball mill accelerant
<b>CA</b>	Citric acid
<b>CSD</b>	Calcium sulfate dihydrate
<b>HH</b>	Calcium sulfate hemihydrate
<b><math>k_g</math></b>	Rate of crystal growth
<b><math>k_n</math></b>	Nucleation rate
<b><math>P_N</math></b>	Probability of nucleation
<b>TrA</b>	Tartaric acid

## 1. Introduction

Calcium sulfate is a very important mineral industrially (principally as the dihydrate, gypsum, and in the anhydrite form). It is used for instance in plasterboard production, dentistry, restorative medicine, and medical plasters.<sup>1,2,11,12,3-10</sup> Three chemically distinct phases exist for the  $\text{CaSO}_4$  – water system at room temperature: the dihydrate (CSD), hemihydrate (HH), and anhydrite.<sup>13</sup> HH comprises two forms ( $\alpha$  and  $\beta$ ), which are structurally identical but have different crystal habits, while there are two structurally different anhydrous forms stable at room temperature ( $\gamma$ -anhydrite and  $\beta$ -anhydrite).

In plasterboard manufacturing, HH is hydrated to give CSD. To ensure that the  $\text{HH} \rightarrow \text{CSD}$  reaction proceeds on a practicable time scale, an additive is often used to control the setting (crystallisation) time of the gypsum product during plasterboard manufacture. The setting time needs to be short enough that the production line length in factories is economical, but not so short that the setting process begins as soon as the hemihydrate and water are mixed (such immediate setting would lead to clogging of the dispensing equipment). Thus, additives in the form of both accelerators and retarders are added to control the setting time.<sup>14</sup> Retarders commonly comprise organic acids such as citric acid, tartaric acid, D,L-malic acid or mesotartaric acid.<sup>15-17</sup> They usually function via adsorption of the acid on the surface of the gypsum crystals, which prevents water adsorption between the grain boundaries of the HH.<sup>18,19</sup>

Any residual water left at the end of the production line is removed by a heat treatment, which is both expensive and time consuming. However, this must be done as an excess of water will lead to a loss of mechanical strength in the final product.<sup>13</sup> This, in addition to the fact that the hydration process from HH to gypsum is inherently rather slow, means that the reaction needs to be accelerated to be industrially viable. By adding seed crystals of gypsum to a slurry of HH and water it is possible to speed up the conversion by providing extra nucleation sites.<sup>20</sup> These seeds are generally prepared using a simple grinding process, which generates large quantities of material but with significant batch-to-batch variation. The product of such milling is termed ball-milled accelerant (BMA), and is composed of raw gypsum mixed with additives such as glycerin, lignin, starch, sugars and a range of salts.<sup>21-24</sup> To avoid issues of interbatch variation in the production of gypsum seeds, the industry has explored a wide range of different materials which might be used to replace BMA, such as  $\text{ZnSO}_4$ , or  $\text{K}_2\text{SO}_4$ .

$\text{ZnSO}_4$  and  $\text{K}_2\text{SO}_4$  are known to be effective accelerants, but the precise effect they have on the HH hydration reaction remains poorly understood. This is because, in general, the plasterboard industry uses indirect methods such as temperature to quantify the setting process.<sup>25</sup> These are simple to implement but offer only limited insight into the setting process. In recent work, we performed a detailed study of the  $\text{HH} \rightarrow \text{CSD}$  hydration process using time-resolved in situ X-ray diffraction, and

were able to provide significant additional insight into the reaction.<sup>26</sup> The use of the non-invasive X-ray probe revealed that the HH hydration reaction is profoundly affected by the presence of BMA. A continuous increase in the nucleation rate,  $k_n$ , with the amount of BMA in the formulation was observed. There is also a general tendency for  $k_g$ , the rate of crystal growth, to rise with increasing BMA concentrations.<sup>26</sup>

In this work, we build on our previous study to explore the effect of the accelerants  $ZnSO_4$  and  $K_2SO_4$  and the retarders  $Na_3PO_4$ , citric acid and tartaric acid on the HH hydration reaction. To do this, we use time-resolved synchrotron X-ray diffraction, which permits us to obtain extensive new insights into the reaction kinetics and mechanisms.

## 2. Methods

### 2.1. Materials

$\alpha$ -HH,  $\beta$ -HH,  $ZnSO_4$ ,  $K_2SO_4$ ,  $Na_3PO_4$ , citric acid (CA) and tartaric acid (TrA) were all obtained from the Etex Group (Avignon, France). Water was deionized before use.

### 2.2. In situ experiments

Beamline I12 (JEEP) at the Diamond Light Source was used to perform time-resolved X-ray diffraction (XRD) measurements. Monochromated X-rays were employed ( $\lambda = 0.2296 \text{ \AA}$ ; energy = 55.012 keV). To calculate the wavelength a previously described protocol was followed.<sup>27</sup> A Thales Pixium RF4343 detector was used to collect XRD patterns. The distance between the sample and detector was 1635.77 mm. Experiments were performed using a PlexiGlas cell built in house (1 cm x 6 cm x 12 cm) and described in a previous report.<sup>26</sup>

In each experiment the cell was loaded with HH (39 g for  $\alpha$ -HH or 31.25 g for  $\beta$ -HH), together with  $ZnSO_4$ ,  $K_2SO_4$ ,  $Na_3PO_4$ , CA or TrA. The holder was placed in an experimental hatch and a homogenizer (Heidolph 741) was installed above it. A pump was also set up above the cell, and a thermocouple inserted into the dry powder. Before adding any water to the HH a few diffraction patterns were collected of the dry powder. The pump was then used to dispense water (17 mL for  $\alpha$ -HH and 25 mL for  $\beta$ -HH) into the sample holder, the homogenizer was switched on, and the slurry stirred at 2000 RPM for 2 min. Throughout the hydration process, XRD patterns were collected every 5 s (4.8 s collection time) until no further changes were observed.

XRD data were collected as 2D Pixium images and azimuthal integration undertaken using the Dawn Workbench (version 2.5.0), followed by background subtraction. The patterns were investigated with

TOPAS Academic (version 5). The peak shapes were fitted with Gaussian functions and the background with Chebyshev functions. Rietveld refinements were performed using the Inorganic Chemistry Structural Database (ICSD) entries 262106 (C2 crystal structure) for HH and 15982 (C2/c crystal structure) for CSD, based on a detailed analysis performed in our previous work.<sup>26</sup> Lattice parameters were refined and phase fractions calculated. The latter were used to determine the percentage of each phase (HH and CSD) present and the extent of reaction.

### 2.3. Kinetic models

A range of kinetic models were explored (**Table S 1**). The induction time was determined using the Avrami-Erofe'ev model (**Equation 1** and **Equation 2**).  $\alpha$  is the extent of the reaction (equivalent to the normalised conversion percentage),  $n$  a reaction exponent which gives information on the mechanism of the reaction,  $k$  the rate constant,  $t$  the elapsed time and  $t_0$  the induction time.

$$\alpha = 1 - e^{-k(t-t_0)^n}$$

**Equation 1.**

$$\ln(-\ln(1 - \alpha)) = n \ln k + n \ln (t - t_0)$$

**Equation 2.**

The Gualtieri model<sup>28</sup> expresses the crystal growth process as detailed in **Equation 3**.

$$\alpha = \frac{1}{1 + \exp\left\{-\left(\frac{t-a}{b}\right)\right\}} \cdot \{1 - \exp[-(k_g t)^n]\}$$

**Equation 3.**

$t$  is the reaction time,  $a$  and  $b$  are parameters related to the nucleation process,  $k_g$  is the rate of crystal growth, and  $n$  is the dimensionality of growth.

SEM images of CSD<sup>29-31</sup> indicate that the crystal habit is needle-like, and hence  $n$  was set to 1 for this analysis. The  $b$  parameter contains information about the crystal growth mechanism, while  $a$  is closely related to the rate of nucleation,  $k_n$  (**Equation 4**).<sup>32</sup>

$$k_n = \frac{1}{a}$$

Equation 4.

a and b can together be used to determine the probability of nucleation,  $P_N$  (Equation 5).<sup>33</sup>

$$P_N = \exp \left\{ -\frac{(t - a)^2}{2b^2} \right\}$$

Equation 5.

### 3. Results

#### 3.1. Time-resolved XRD data

In situ XRD data for the hydration of  $\beta$ -HH in the presence of the accelerator  $K_2SO_4$  are shown in **Figure 1**, with plots for  $ZnSO_4$ ,  $Na_3PO_4$ , CA and TrA given in the Supporting Information (**Figure S 1 - Figure S 4**). Exemplar Rietveld refinements, used to calculate phase fractions, are presented in **Figure S 5 - Figure S 8**. In all cases, after an initial induction time significant changes in the positions of the Bragg reflections are visible (**Figure 1 (a,b)**). These correspond to the conversion of HH to CSD. The  $\beta$ -HH and CSD phase fraction lines cross at 50 % (**Figure 1(c,d)**), indicating that the hydration process is a direct conversion (with no intermediates present). Similar findings were obtained in our previous study using BMA as an accelerant.<sup>26</sup> The maximum temperatures reached by the systems together with the total conversion and the percentage conversion of hemihydrate to dihydrate at the maximum temperature are summarized in **Table 1**. It can be seen that in most cases the maximum temperature reached by the systems is attained before the maximum conversion from HH to CSD. As detailed in **Table 1**, the maximum temperature lies in the region of 24-34 °C. In the presence of  $K_2SO_4$  and  $ZnSO_4$  (as also with BMA) higher temperatures are observed with increasing concentrations of the additives (**Figure 2(a)**). This effect is reversed for system containing  $Na_3PO_4$  and citric acid, as depicted in **Figure 2(b)**. Tartaric acid requires the longest time to reach the maximum temperature, and also results in the lowest temperatures and the smallest percentage of CSD at this temperature (**Figure 2(c)**).

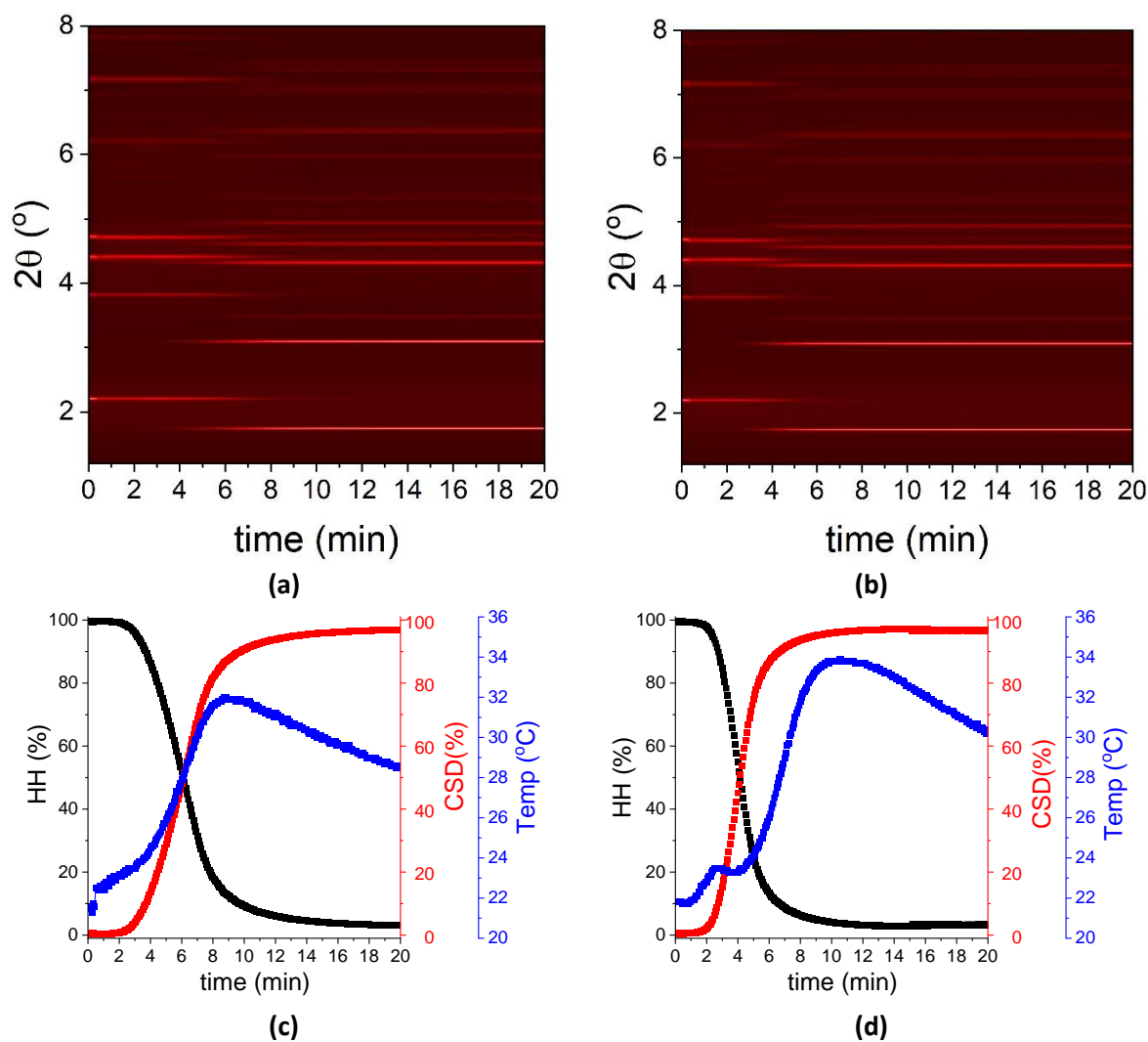


**Figure 1.** Time-resolved data showing the hydration of  $\beta$ -HH supplemented with (a,c) 0.2 % w/v  $K_2SO_4$  and (b,d) 1 % w/v  $K_2SO_4$ . (a) and (b) depict contour plots of the XRD data as a function of time. (c) and (d) are phase fractions of the HH and CSD determined by batch Rietveld refinements and plotted in percentage terms.

The total conversion never reaches 100 % for any of the systems presented here, as was also observed for the system containing BMA,<sup>26</sup> and instead lies between 93-98 % (Figure 2). It is clear (Table 1) that  $K_2SO_4$  is a potent accelerator, reaching 50% and maximum conversion more rapidly than an equivalent concentration of BMA or when the system has no additive at all.  $ZnSO_4$  is also effective as an accelerant. All other additives such as  $Na_3PO_4$ , citric acid and tartaric acid have times to reach 50 % conversion in range 11 to 49 min (5 – 7 min for BMA). The time to reach max conversion is shorter for  $K_2SO_4$  and  $ZnSO_4$  than for systems containing BMA or no additive.

**Table 1.** Descriptive data on the  $\beta$ -HH to CSD conversion for systems with different additives. Data for BMA is from previous publication. CA: citric acid; TrA: tartaric acid.

System	Maximum temp. (°C)	Time to reach 50% conversion (min)	Time to reach max. temp. (min)	Time to reach max. conversion (min)	Conversion at max. temp. (%)	Total conversion (%)
No additive	31	6	46	75	80	95
BMA 0.2 % w/w <sup>26</sup>	28	7	14	50	94	98
BMA 1 % w/w <sup>26</sup>	30	5	10	30	77	97
K <sub>2</sub> SO <sub>4</sub> 0.2 % w/w	32	6	9	17	87	97
K <sub>2</sub> SO <sub>4</sub> 1 % w/w	34	4	11	11	96	97
ZnSO <sub>4</sub> 0.2 % w/w	28	11	39	22	97	97
ZnSO <sub>4</sub> 1 % w/w	30	11	33	26	97	97
Na <sub>3</sub> PO <sub>4</sub> 0.05 % w/w	27	17	22	91	67	96
Na <sub>3</sub> PO <sub>4</sub> 0.2 % w/w	28	37	66	62	97	97
Na <sub>3</sub> PO <sub>4</sub> 0.5 % w/w	26	49	62	80	94	97
CA 0.1 % w/w	28	52	58	78	91	96
CA 0.5 % w/w	24	222	232	240	66	95
TrA 0.1% w/w	24	267	287	381	57	93

All the above reactions were performed with  $\beta$ -HH. For comparison, we also explored the use of 0.1 % w/w citric acid in the hydration of  $\alpha$ -HH (see **Table 2**). Here, the maximum temperature of the system is very close to that observed for  $\alpha$ -HH (with no additive) and slightly lower than for the system with 0.2% BMA. The total conversion for all the systems (no additive, BMA or CA) is exactly the same and stands at 98%. The times needed to reach the 50% conversion, the maximum temperature and maximum conversion are much higher for the CA system than with no additive or in the presence of BMA. This is expected as the citric acid acts as a retardant.<sup>34</sup>

**Table 2.** Descriptive data on the  $\alpha$ -HH to CSD conversion.

System	Maximum temp. (°C)	Time to reach 50% conversion (min)	Time to reach max. temp. (min)	Time to reach max. conversion (min)	Conversion at max. temp. (%)	Total conversion (%)
No additive	27	18	36	45	94	98
BMA 0.2 % w/w	30	16	31	45	92	98
CA 0.1 % w/w	26	115	139	150	95	98

When we look at the data for 0.1% w/w CA with  $\alpha$ -HH (**Table 1**) and  $\beta$ -HH (**Table 2**) we can see that CA causes the system to have a lower maximum temperature than for the systems with no additive or BMA, much longer times to reach 50% conversion and reduced maximum conversion percentages. This is consistent with the retardant properties of CA.<sup>34</sup> It seems that CA has stronger retardant properties with  $\beta$ -HH, as the times recorded are much longer than in the  $\alpha$ -HH system. This could be

due to the fact that  $\beta$ -HH has usually much more smaller particles and therefore CA will block more nucleation sites.<sup>35,36</sup>

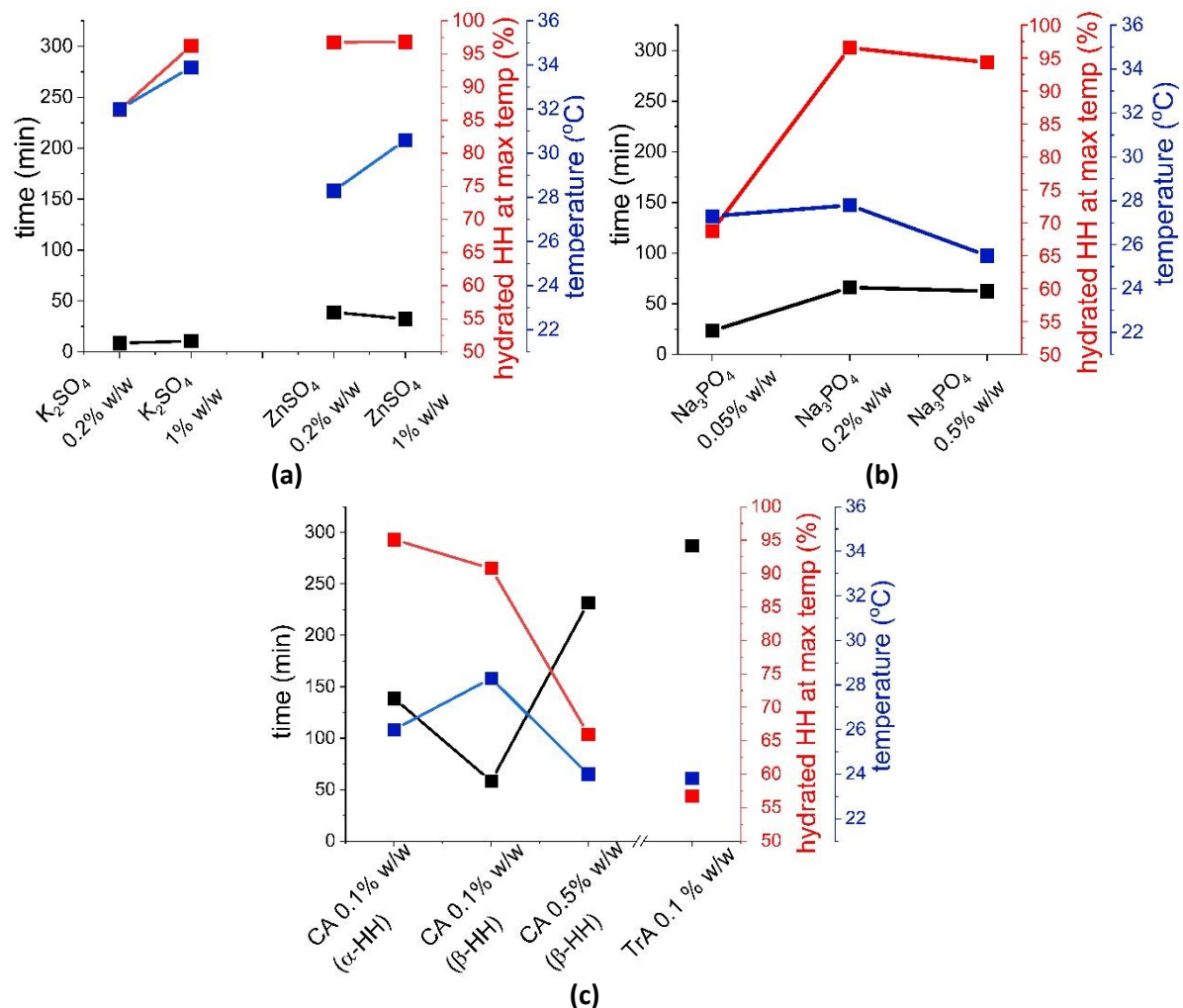


**Figure 2.** Data for the hydration of  $\beta$ -HH in the presence of (a)  $K_2SO_4$  and  $ZnSO_4$ ; (b)  $Na_3PO_4$ ; and (c) CA and TrA, showing the time taken to reach the maximum temperature and the percentage conversion at which the temperature peaks.

When we look at the times needed to reach 90-94 % of total conversion for  $\beta$ -HH, three distinctive groups are visible (**Figure 3**). Additives which work as accelerators ( $BMA$ ,  $K_2SO_4$  and  $ZnSO_4$ ) lead to reduced conversion times in the region of 5 - 20 min. There is then a second group of data where 40 - 65 min is required; here, the additives are having little effect on the process, and the times are similar to HH alone ( $Na_3PO_4$ , low concentration CA). The third set of plots correspond to strong retardants (high concentration CA and TrA), where > 200 min is required to reach these high conversion percentages.

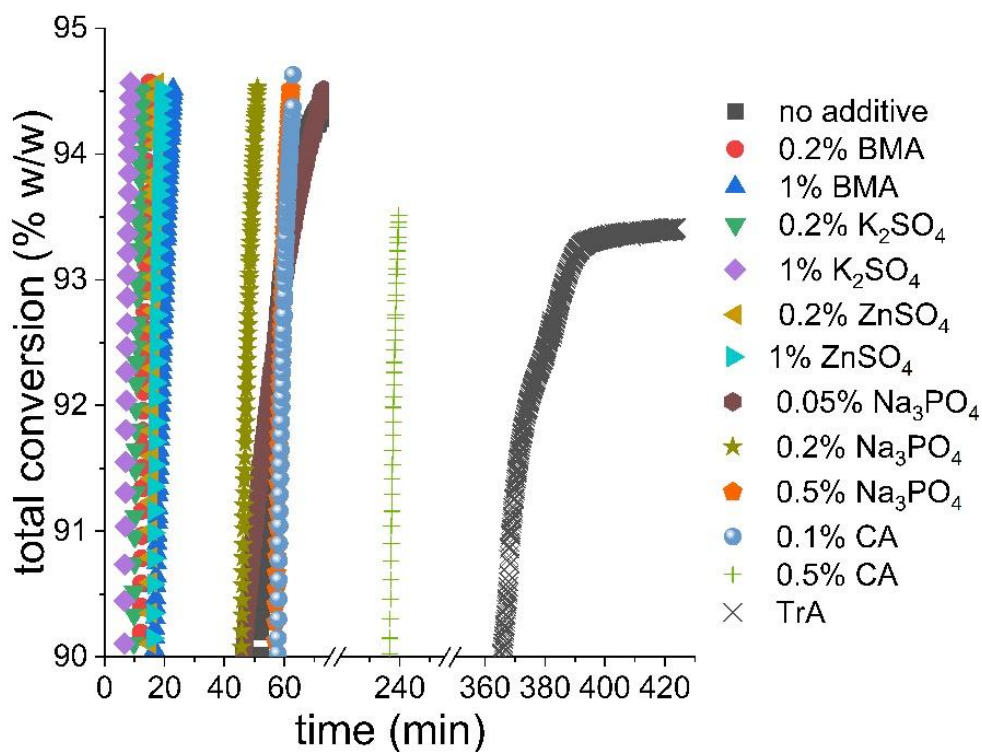
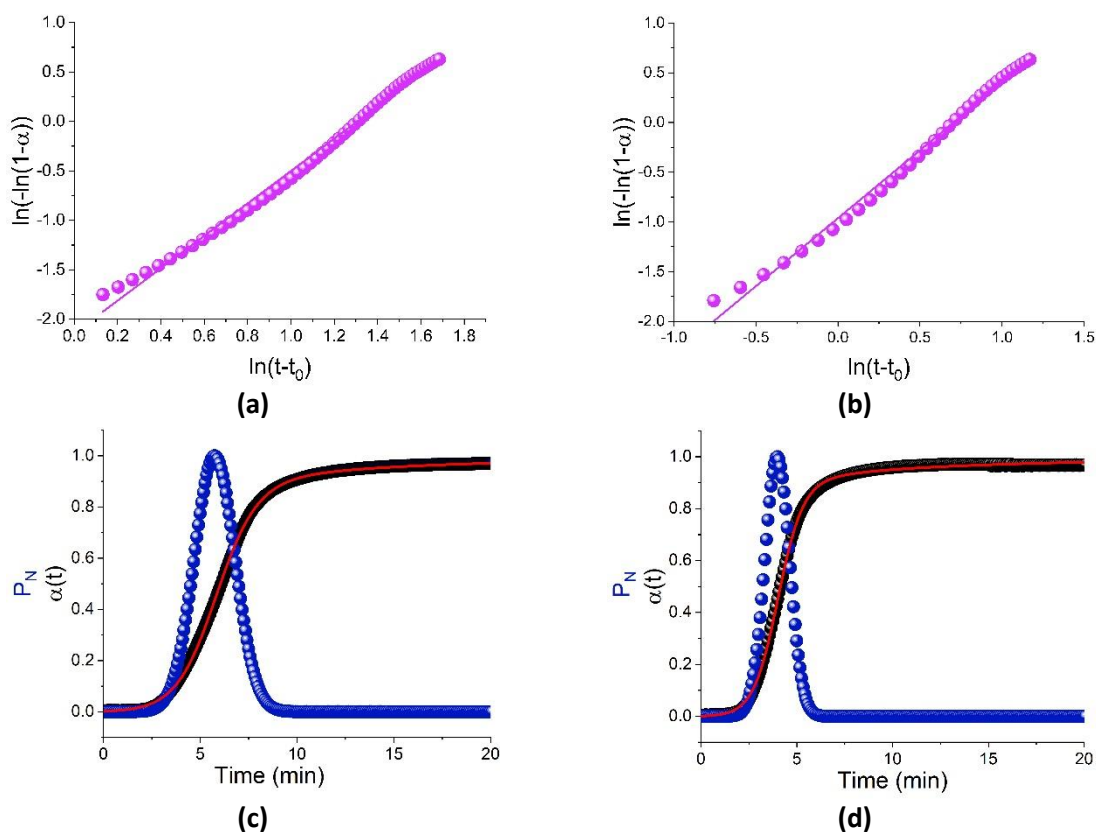


Figure 3. A plot showing the final stages of the HH to CSD hydration.

### 3.2. Kinetic modelling

#### 3.2.1. Potassium sulfate

To understand the reactions in more detail, we attempted to apply a range of kinetic models to the hydration reactions. As seen in **Table S 2** and **Table S 3** (see also **Figure S 9** and **Figure S 10**) the fitting is poor for all the kinetic models except for the Avrami-Erofe'ev and Gualtieri models (**Figure 4**).



**Figure 4.** The results of fitting the (a-b) Avrami-Erofe'ev model; and (c-d) Gualtieri model to the hydration of HH in the presence of (a, c) 0.2% and (b, d) 1% w/w  $K_2SO_4$ . In (c,d) experimental data (■), the corresponding Gualtieri fits (—) and the calculated rate of nucleation ( $P_N$ ; ●) are depicted.

The parameters determined from Avrami-Erofe'ev kinetic model fitting are given in **Table 3**.

**Table 3.** Kinetic parameters calculated from Sharp-Hancock and Gualtieri plots for  $K_2SO_4$  accelerated reactions.

Sharp-Hancock model				
Sample	$k$ ( $\text{min}^{-1}$ )	$n$	$t_0$ (min)	
No additive	$1.33 \times 10^{-5} \pm 0.07 \times 10^{-5}$	$3.24 \pm 0.02$	$8.91 \pm 1.85$	
BMA 0.2% w/w	$1.92 \times 10^{-5} \pm 0.05 \times 10^{-2}$	$2.10 \pm 0.02$	$1.98 \pm 0.24$	
BMA 1% w/w	$2.71 \times 10^{-2} \pm 0.32 \times 10^{-2}$	$0.85 \pm 0.01$	$2.60 \pm 0.02$	
$K_2SO_4$ 0.2% w/w	$0.118 \pm 0.003$	$1.64 \pm 0.02$	$3.02 \pm 0.10$	
$K_2SO_4$ 1% w/w	$0.382 \pm 0.006$	$1.37 \pm 0.02$	$2.53 \pm 0.06$	
Gualtieri model				
	$a$ (min)	$b$ (min)	$k_g$ ( $\text{min}^{-1}$ )	
			$k_n$ ( $\text{min}^{-1}$ )	
No additive	$34.80 \pm 0.07$	$5.48 \pm 0.05$	$0.05 \pm 0.00$	$0.03 \pm 0.00$
BMA 0.2% w/w	$6.30 \pm 0.05$	$1.52 \pm 0.04$	$0.19 \pm 0.00$	$0.16 \pm 0.01$
BMA 1% w/w	$3.03 \pm 0.04$	$0.83 \pm 0.04$	$0.15 \pm 0.00$	$0.33 \pm 0.01$
$K_2SO_4$ 0.2% w/w	$5.87 \pm 0.01$	$1.08 \pm 0.01$	$8.18 \pm 1.40$	$0.17 \pm 0.00$
$K_2SO_4$ 1% w/w	$4.01 \pm 0.01$	$0.66 \pm 0.01$	$4.42 \pm 0.69$	$0.25 \pm 0.00$

The addition of  $K_2SO_4$  reduces the induction time, and also lowers the value of the reaction exponent in the Avrami model. It is not clear precisely what the changes in exponent correspond to in terms of the reaction mechanism, since a number of different possibilities would be consistent with the observed  $n$  values.<sup>37</sup> However, it does appear that the importance of nucleation is diminished in the presence of  $K_2SO_4$  and BMA. The value of the rate constant increases two-fold with the increase of  $K_2SO_4$  concentration and 29,000-fold if compared with no additive system.

Considering the Gualtieri fits (**Table 3**) the addition of  $K_2SO_4$  is seen to increase both the rate of nucleation ( $k_n$ ) and the rate of crystal growth ( $k_g$ ) over the additive-free reaction. This was also observed for systems with BMA.<sup>26</sup> The increase in  $k_g$  is much greater with  $K_2SO_4$ , while the changes in  $k_n$  are similar to those with BMA.  $k_g$  is greater than  $k_n$  for both the systems containing  $K_2SO_4$ , which indicates that nucleation is the rate limiting process. With  $K_2SO_4$ -accelerated reactions, the increase in  $k_n$  is continuous with a rise in the seed concentration, whereas  $k_g$  is highest with 0.2 % w/w seeds. This is different to the trend with BMA, where  $k_n$  becomes greater with the increased concentration of seeds.  $K_2SO_4$  can both act as seeds on which CSD growth can occur (increasing  $k_n$ ) and also provide extra feedstock (in the form of sulfate ions, since  $K_2SO_4$  is more soluble than  $CaSO_4$ ) for the growth of the crystals (raising the value for  $k_n$ ). The data indicate that the latter is more important at lower concentrations of seeds, and the former more important at higher concentrations. The  $b$  parameters are all much smaller than 15 min, indicating that nucleation is heterogeneous, as would be expected for a seeded system.<sup>38</sup> The values of  $a$  and  $b$  decrease with an increase in the amount of  $K_2SO_4$ , as here crystallization can take place at a greater number of preformed aggregates in the reaction. The  $a$  value is directly connected with  $k_n$  value, and thus the reduction here with increasing  $K_2SO_4$  is expected. The  $b$  parameter is below 15 min in all cases, indicating heterogenous nucleation.

### 3.2.2. Zinc sulfate

Fitting of kinetic models to the  $ZnSO_4$  data (**Table S 4 - Table S 5; Figure S 11 - Figure S 12**) is generally poor, except in the case of the Gualtieri model as shown in **Figure 5**. The fits here are as good as for the  $K_2SO_4$  systems.

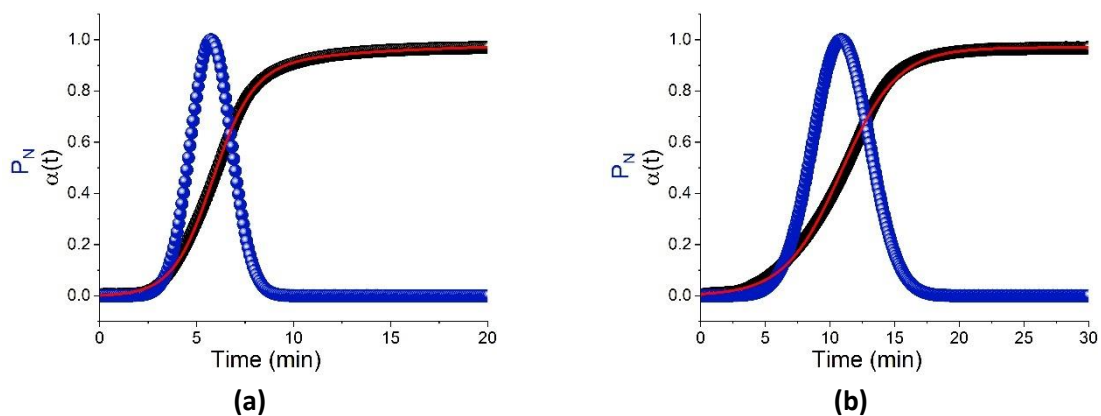


**Figure 5.** Gaultieri fits for the hydration of  $\beta$ -HH with (a) 0.2% w/w  $\text{ZnSO}_4$ ; and (b) 1% w/w  $\text{ZnSO}_4$ ; Experimental data (■), the corresponding Gaultieri fits (—) and the calculated rate of nucleation ( $P_N$ ; ●) are depicted.

The parameters calculated from the Gaultieri kinetic model are given in **Table 4**:

**Table 4.** Kinetic parameters calculated from Gaultieri plots for  $\text{ZnSO}_4$  accelerated reactions.

Sample	a (min)	b (min)	$k_g$ ( $\text{min}^{-1}$ )	$k_n$ ( $\text{min}^{-1}$ )
$\text{ZnSO}_4$ 0.2% w/w	$10.50 \pm 0.01$	$1.94 \pm 0.01$	$5.97 \times 10^{34} \pm 4.04 \times 10^{36}$	$0.100 \pm 0.00$
$\text{ZnSO}_4$ 1% w/w	$10.90 \pm 0.01$	$2.17 \pm 0.01$	$2.98 \times 10^2 \pm 5.66 \times 10^{-4}$	$0.090 \pm 0.00$

Even though the Gaultieri fit is good (**Figure 5**) the calculated parameters (**Table 4**) do not allow for definitive conversions to be reached. In both cases  $b < 15$  min, which is indicative of heterogeneous nucleation. It appears that  $k_g$  increases enormously with addition of  $\text{ZnSO}_4$  while  $k_n$  stays almost the same (as does the a-parameter). The rate of crystal growth is higher than the rate of nucleation (for both  $\text{ZnSO}_4$  concentration) indicating nucleation is the rate limiting process (where for BMA and  $\text{K}_2\text{SO}_4$  the limiting rate depends on concentration). Solubility in water (20 °C) for  $\text{ZnSO}_4$  is 35 (wt %) and for  $\text{K}_2\text{SO}_4$  is 9.95 (wt %),<sup>39</sup> which allows us to explain these findings: the increased solubility of Zn sulfate provides an increased feedstock of ions with which to contrast a lattice, and thus leads to a rise in  $k_g$ . However, the high solubility also results in relatively few additional nucleation sites, resulting in only a modest increase in  $k_n$  over the additive-free reaction.

### 3.2.3. Sodium phosphate

Poor fits of the kinetic models were obtained when sodium phosphate was added to the system (see **Figure S 13 - Figure S 15; Table S 6 - Table S 8**). The Gaultieri model fits well when the concentration of  $\text{Na}_3\text{PO}_4$  is small (0.05 % w/w) (**Figure 6(a)**), but the fit becomes much worse at higher concentrations

(0.2 % and 0.5 % w/w), as shown in **Figure 6 (b-c)**. It is clear that the  $P_N$  maximum is shifting to later times with an increased  $\text{Na}_3\text{PO}_4$  concentration (**Figure 6**), suggesting an increased induction time.

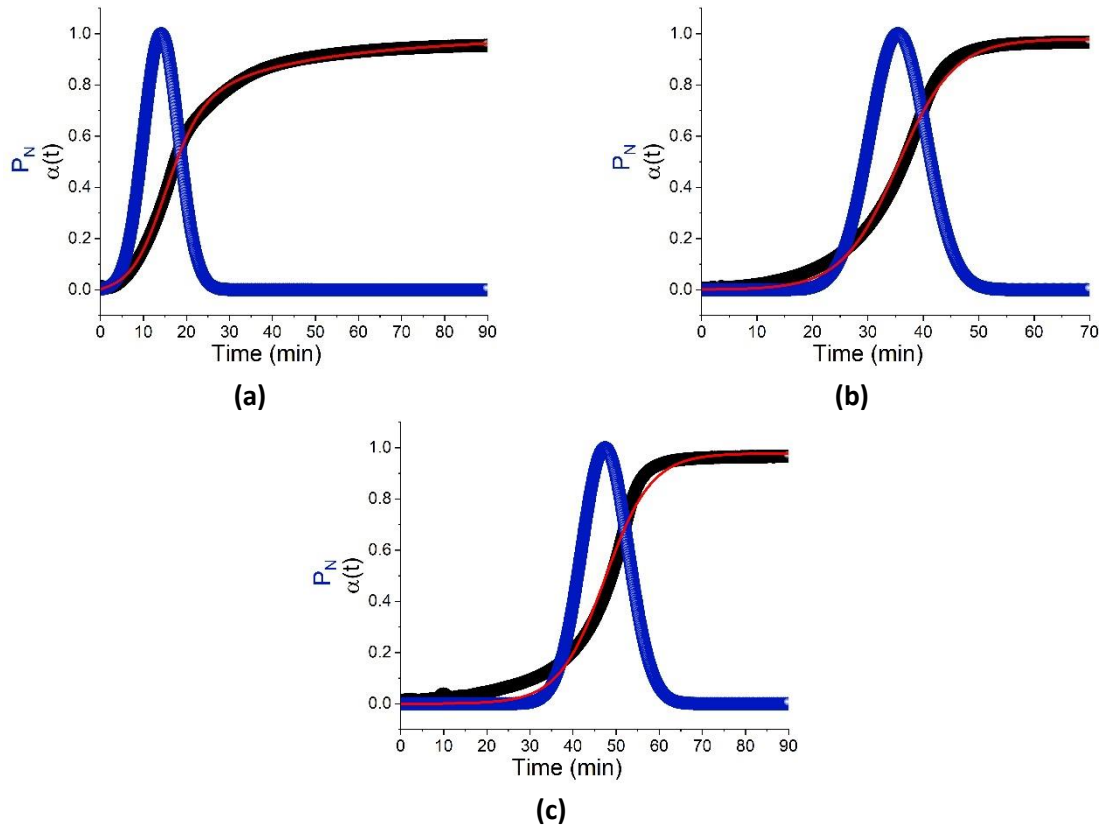


**Figure 6.** Gualtieri fits for the hydration of  $\beta$ -HH in the presence of **(a)** 0.05 %; **(b)** 0.2 %; and **(c)** 0.5 % w/w  $\text{Na}_3\text{PO}_4$ . Experimental data (■), the corresponding Gualtieri fits (—) and the calculated rate of nucleation ( $P_N$ ; ●) are depicted.

Given the poor quality of fits and large errors in many of the kinetic parameters calculated with  $\text{Na}_3\text{PO}_4$  it is not possible to draw any clear conclusions. The retardant properties could be due to the fact that some of the sulfate ions in the CSD crystal lattice are replaced with the phosphate ions, which results in inhibition of the growth of the crystals. The crystallization of gypsum in the presence of phosphate is known to yield a stable material, ardealite ( $\text{Ca}_2\text{HPO}_4\text{SO}_4 \cdot 4\text{H}_2\text{O}$ ), and the formation of this presumably competes with CSD formation and inhibits further precipitation.<sup>40</sup> The crystallization of gypsum in the presence of phosphate is known to yield a stable material, ardealite ( $\text{Ca}_2\text{HPO}_4\text{SO}_4 \cdot 4\text{H}_2\text{O}$ ), and the formation of this presumably competes with CSD formation and inhibits further precipitation.<sup>41,42</sup>

### 3.2.4. Citric acid and tartaric acid

The fitting of different kinetic models to these reactions are presented in **Figure S 16 - Figure S 19**, with  $R^2$  values shown in **Table S 9 - Table S 12**. The fits in all cases are poor, and hence we are unable to deduce any further insight for these systems.

## 4. Discussion

Overall, it appears that the addition of both accelerants and retardants causes profound changes in the HH hydration process. With citric acid and tartaric acids, the reaction mechanism is found to be too complex to model with standard kinetic models. Even where the models could be fitted, often the parameter values obtained fall out with those previously reported. The  $k_n$  and  $k_g$  values for the systems with low concentrations of  $K_2SO_4$  lie within the range reported by previous studies ( $0.019 < k_n < 0.72 \text{ min}^{-1}$  and  $0.00034 < k_g < 9.9 \times 10^5 \text{ min}^{-1}$ ).<sup>26</sup> For the remainder of the systems at least one of the parameters is out of the previously recorded range.

The literature generally shows an increase in both  $k_n$  and  $k_g$  with the temperature of the reaction.<sup>28,32,43</sup> Here, we see an increase in the nucleation rate,  $k_n$ , with the amount of  $K_2SO_4$ ; with  $ZnSO_4$   $k_n$  is greater than the unaccelerated value at both concentrations studied, but there is minimal difference between the 0.2 and 1 % w/w systems. This is consistent with the reduced importance of nucleation in controlling reaction rate implied from fits of the Avrami-Erofe'ev model to the data where those could be obtained.  $k_g$  is much greater than the unaccelerated value with both  $K_2SO_4$  and  $ZnSO_4$  concentrations, but seems to be lower at higher concentrations. This differs from the data obtained for BMA where both  $k_g$  and  $k_n$  generally increase with concentration.<sup>26</sup>  $k_g$  is much greater than  $k_n$  in all cases with  $K_2SO_4$  and  $ZnSO_4$ , while for BMA the values are much more comparable.

We should note that, while the Avrami and Gualtieri models provide useful insight into the reaction process, both have some limitations, since they are designed for systems where crystallization takes place in a homogenous medium that contains the species required for nucleation. There will inevitably be some degree of heterogeneity in the water/HH system, and thus the models could miss some additional complexity.

The creation of a new crystalline unit from a solution starts with the nucleation process. Nucleation is defined as a series of processes by which the atoms, ions or molecules of a solution or melt rearrange into a cluster of the product phase large enough to be able to grow permanently to a macroscopically larger size.<sup>44</sup> The cluster is defined as the nucleus.<sup>44</sup> Nucleation can be homogeneous, in the absence of foreign elements or crystals in the solution, or heterogeneous, in the presence of foreign elements

in the solution (accelerators or retardants). Both types of nucleation are together termed primary nucleation. Secondary nucleation takes place when nucleation is induced by the presence of crystals of the same material (e.g. BMA).<sup>45</sup> The use of CSD seeds to accelerate the HH → CSD hydration process is thus a secondary nucleation phenomenon. Following nucleation, there is crystal growth, in which an atom, ion or molecule is deposited onto the surface of a nucleus, causing an increase in size.<sup>45</sup> The crystal growth process can be summarized into four steps (**Figure 7**).

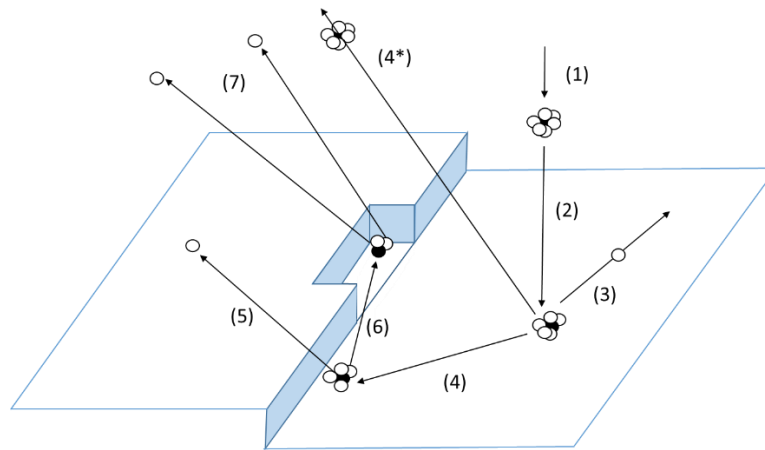


**Figure 7.** Schematic representation of the processes involved in crystal growth: (1) Transport of solute to a position near the crystal surface; (2) diffusion through the boundary layer; (3) adsorption onto the crystal surface; (4) diffusion over the surface; (4\*) desorption from the surface; (5) attachment to a step or edge; (6) diffusion along the step or edge; (7) Incorporation into a kink site or step vacancy. Adopted from reference<sup>45</sup>

In the first step, the solute is transported near the crystal structure (1), after which diffusion through the boundary layer takes place (2). Adsorption then occurs onto the crystal surface (3), together with diffusion over the surface (4). At the same time, desorption from the surface can also happen (4\*). In the next step, attachment to a step or edge occurs (5) followed by diffusion along the step or edge (6). In the final step, the incorporation into a kink site or step vacancy is seen (7). There are thus two distinct elements of crystal growth: the transport process (step 1) and surface processes (steps 3-7). The slowest process will control the overall crystal growth rate, which can be transport controlled (step 1) or surface controlled (steps 3-7).<sup>45</sup>

Considering the accelerants  $K_2SO_4$  and  $ZnSO_4$ , the seed particles can both affect crystal nucleation (by providing primary nucleation sites on which CSD can grow) and growth (by dissolving into solution to provide a supply of  $SO_4^{2-}$ ). This perhaps explains why the trends in terms of changes in  $k_g$  and  $k_n$  are complex: the balance of these effects varies with the amount of seed material present. In the case of  $Na_3PO_4$  the situation is even more complex because of the potential to form ardealite as a byproduct

during the reaction. The retardant CA is known to be preferentially adsorbed on the surface of the c-axis and slows down its growth.<sup>46</sup> The same principle is expected to apply for TrA. These effects are clear from the increased induction time and times to reach 50 % and maximum conversion noted with these materials (**Table 1**). However, the reason why this inhibition also translates to standard kinetic models not fitting the data is not clear. It is possible that the selective inhibition of growth in one direction renders the crystal growth sufficiently anisotropic for simple models to be insufficiently sophisticated, but this requires more detailed investigation.

## 5. Conclusions

A detailed study of the hydration of  $\text{CaSO}_4 \cdot 0.5\text{H}_2\text{O}$  in the presence of commercially relevant additives was undertaken in this work using time-resolved synchrotron X-ray diffraction. The temperature is found to be a poor proxy for the extent of reaction, with the maximum temperature reached well before the reaction is complete. Fitting kinetic models to the time-resolved data revealed that the Avrami-Erofe'ev and Gualtieri models provide the best description of the experimental findings. The addition of accelerants is seen to reduce the importance of nucleation in determining the reaction rate, and to increase the rate of reaction. In the Gualtieri model, all the accelerants  $\text{K}_2\text{SO}_4$ ,  $\text{ZnSO}_4$  or BMA increase  $k_g$  and  $k_n$  above the unaccelerated system, but have markedly different effects. This is believed to be connected to the solubility of the accelerants used, with more soluble species able to provide an increased concentration of ions in solution to act as feedstock, hence having a greater effect on  $k_g$  than  $k_n$ , while less soluble analogues act mainly through  $k_n$ . In the case of the retardant species, none of the kinetic models provided a good fit to the data, suggesting that the effect of these additives is very complex and cannot be modelled with the existing paradigms.

## 6. Acknowledgements

The authors gratefully acknowledge the Etex Group for funding this research, and the Diamond Light Source for access to Beamline I12 (experiment EE-16022-1). We also thank Dr. Oxana Magdysyuk for assistance with *in situ* experiments and Mr John Frost for manufacturing the cells used for time-resolved studies.

## 7. References

- (1) Kim, D. H.; Jenkins, B. M.; Oh, J. H. Gypsum Scale Reduction and Collection from Drainage Water in Solar Concentration. *Desalination* **2011**, *265* (1–3), 140–147. <https://doi.org/10.1016/j.desal.2010.07.044>.
- (2) Thomas, G. Thermal Properties of Gypsum Plasterboard at High Temperatures. *Fire Mater.* **2002**, *26* (1), 37–45. <https://doi.org/10.1002/fam.786>.
- (3) Kumar, S. R.; Bhat, I. K.; Patnaik, A. Novel Dental Composite Material Reinforced with Silane Functionalized Microsized Gypsum Filler Particles. *Polym. Compos.* **2017**, *38* (2), 404–415. <https://doi.org/10.1002/pc.23599>.
- (4) Alexopoulou, M.; Mystiridou, E.; Mouzakis, D.; Zaoutsos, S.; Fatouros, D. G.; Bouropoulos, N. Preparation, Characterization and in Vitro Assessment of Ibuprofen Loaded Calcium Phosphate/Gypsum Bone Cements. *Cryst. Res. Technol.* **2016**, *51* (1), 41–48. <https://doi.org/10.1002/crat.201500143>.
- (5) Zmurko, M. G.; Belkoff, S. M.; Herzenberg, J. E. Mechanical Evaluation of a Soft Cast Material. *Orthopedics* **1997**, *20* (8), 693–698.
- (6) Jubayer, M. F.; Uddin, M. B.; Faruque, M. O. Standardization Parameters for Production of Tofu Using WSD-Y-1 Machine. *J. Bangladesh Agril. Univ.* **2013**, *11* (2), 307–312.
- (7) Mé, Y.; Lanos, C.; Nguyen, K. S.; Daiguebonne, C.; Guillou, O.; Freslon, S. One-Dimensional-Time Study of the Dehydration of Plasterboards Under Standard Fire Condition (ISO 834): Thermo-Chemical Analysis. *J. Fire Sci.* **2010**, *29* (4), 299–316. <https://doi.org/10.1177/0734904110391889>.
- (8) Fu, L.; Xia, W.; Mellgren, T.; Moge, M.; Engqvist, H. Preparation of High Percentage Alfa-Calcium Sulfate Hemihydrate via a Hydrothermal Method. *J. Biomater. Nanobiotechnol.* **2017**, *08* (01), 36–49. <https://doi.org/10.4236/jbnb.2017.81003>.
- (9) Parker, A. C.; Smith, J. K.; Courtney, H. S.; Haggard, W. O. Evaluation of Two Sources of Calcium Sulfate for a Local Drug Delivery System: A Pilot Study. *Clin. Orthop. Relat. Res.* **2011**, *469* (11), 3008–3015. <https://doi.org/10.1007/s11999-011-1911-1>.
- (10) Petrone, C.; Magliulo, G.; Manfredi, G. Mechanical Properties of Plasterboards: Experimental Tests and Statistical Analysis. *J. Mater. Civ. Eng.* **2016**, *28* (11), 04016129. [https://doi.org/10.1061/\(asce\)mt.1943-5533.0001630](https://doi.org/10.1061/(asce)mt.1943-5533.0001630).
- (11) Artioli, G.; Bullard, J. W. Cement Hydration: The Role of Adsorption and Crystal Growth. *Cryst. Res. Technol.* **2013**, *48* (10), 903–918. <https://doi.org/10.1002/crat.201200713>.
- (12) López-Delgado, A.; López-Andrés, S.; Padilla, I.; Alvarez, M.; Galindo, R.; José Vázquez, A. Dehydration of Gypsum Rock by Solar Energy: Preliminary Study. *Geomaterials* **2014**, *04* (03), 82–91. <https://doi.org/10.4236/gm.2014.43009>.
- (13) Wirsching, F. *Calcium Sulfate*; Wiley: Weinheim, Germany, 2002; Vol. 92. <https://doi.org/10.1002/3527600418>.
- (14) Lewry, A. J.; Williamson, J. The Setting of Gypsum Plaster. Part III the Effect of Additives and

- Impurities. *J. Mater. Sci.* **1994**, *29* (23), 6085–6090. <https://doi.org/10.1007/BF00354546>.
- (15) Saha, A.; Lee, J.; Pancera, S. M.; Bräeu, M. F.; Kempter, A.; Tripathi, A.; Bose, A. New Insights into the Transformation of Calcium Sulfate Hemihydrate to Gypsum Using Time-Resolved Cryogenic Transmission Electron Microscopy. *Langmuir* **2012**, *28* (30), 11182–11187. <https://doi.org/10.1021/la3024474>.
- (16) Hill, J.-R.; Plank, J. Retardation of Setting of Plaster of Paris by Organic Acids: Understanding the Mechanism through Molecular Modeling. *J. Comput. Chem.* **2004**, *25* (12), 1438–1448. <https://doi.org/10.1002/jcc.20070>.
- (17) Gilbert, R. L. Crystallization of Gypsum in Wet Process Phosphoric Acid. *Ind. Eng. Chem. Process Des. Dev.* **1966**, *5* (4), 388–391. <https://doi.org/10.1021/i260020a008>.
- (18) Lanzón, M.; García-Ruiz, P. A. A. Effect of Citric Acid on Setting Inhibition and Mechanical Properties of Gypsum Building Plasters. *Constr. Build. Mater.* **2012**, *28* (1), 506–511. <https://doi.org/10.1016/j.conbuildmat.2011.06.072>.
- (19) Magallanes-Rivera, R. X.; Escalante-García, J. I.; Gorokhovskiy, A. Hydration Reactions and Microstructural Characteristics of Hemihydrate with Citric and Malic Acid. *Constr. Build. Mater.* **2009**, *23* (3), 1298–1305. <https://doi.org/10.1016/j.conbuildmat.2008.07.022>.
- (20) Amathieu, L.; Boistelle, R. Improvement of the Mechanical Properties of Set Plasters by Means of Four Organic Additives Inducing {101} Faces. *J. Cryst. Growth* **1986**, *79* (1–3), 169–177. [https://doi.org/10.1016/0022-0248\(86\)90432-X](https://doi.org/10.1016/0022-0248(86)90432-X).
- (21) Otto L. Dozsa. Accelerator for Gypsum Plaster and Process of Manufacture - US4681644, 1987.
- (22) Campbell, F. H.; Piasecki, R. J.; Kingston, L. W.; Burkard, E. A. Gypsum Set Accelerator and Method of Making the Same Patent: US 6221151 B1, 2001.
- (23) Immordino, S. C.; Espinoza, T.; Stevens, R. B.; Miller, C. J. Efficient Set Accelerator for Plaster Patent: US 6379458, 2002.
- (24) Campbell, Frank, H.; Piasecki, Robert, J.; Kingston, Larry, W.; Burkard, Edward, A. Method of Making a Gypsum Set Accelerator - Patent EP 1 204 614 B1. EP 1 204 614 B1, 2004.
- (25) Lewry, A. J.; Williamson, J. The Setting of Gypsum Plaster - Part I The Hydration of Calcium Sulphate Hemihydrate. *J. Mater. Sci.* **1994**, *29* (20), 5279–5284. <https://doi.org/10.1007/BF01171536>.
- (26) Gurgul, S. J.; Seng, G.; Williams, G. R. A Kinetic and Mechanistic Study into the Transformation of Calcium Sulfate Hemihydrate to Dihydrate. *J. Synchrotron Radiat.* **2019**, *26* (3), 774–784. <https://doi.org/10.1107/S1600577519001929>.
- (27) Hart, M. L.; Drakopoulos, M.; Reinhard, C.; Connolly, T. Complete Elliptical Ring Geometry Provides Energy and Instrument Calibration for Synchrotron-Based Two-Dimensional X-Ray Diffraction. *J. Appl. Crystallogr.* **2013**, *46* (5), 1249–1260. <https://doi.org/10.1107/S0021889813022437>.
- (28) Gualtieri, A. F. Synthesis of Sodium Zeolites from a Natural Halloysite. *Phys. Chem. Miner.* **2001**, *28* (10), 719–728. <https://doi.org/10.1007/s002690100197>.

- (29) Sirota, I. S.; Dorozhkin, S. V.; Kruchinina, M. V.; Melikhov, I. V. Phase Transformation and Dehydration of Calcium Sulphate Dihydrate in Solution Studied by SEM. *Scanning* **1992**, *14* (5), 269–275. <https://doi.org/10.1002/sca.4950140505>.
- (30) Polat, S.; Sayan, P. Determination of the Effects of Carboxylic Acids on Calcium Sulfate Dihydrate Crystallization. *Chem. Eng. Technol.* **2017**, *40* (7), 1354–1361. <https://doi.org/10.1002/ceat.201600525>.
- (31) Zhang, Y.; Deng, L.; Chen, F.; Cao, S.; You, S.; Liu, Y.; Zhang, Y. Reactive Crystallization of Calcium Sulfate Dihydrate from Acidic Wastewater and Lime. *Chinese J. Chem. Eng.* **2013**, *21* (11), 1303–1312. [https://doi.org/10.1016/S1004-9541\(13\)60626-6](https://doi.org/10.1016/S1004-9541(13)60626-6).
- (32) Etampawala, T.; Mull, D. L.; Keum, J. K.; Jenkins, D. M.; Dadmun, M. Insights into the Morphology and Kinetics of Growth of Silver Metal-Organic Nanotubes. *Cryst. Growth Des.* **2016**, *16* (3), 1395–1403. <https://doi.org/10.1021/acs.cgd.5b01509>.
- (33) El Osta, R.; Feyand, M.; Stock, N.; Millange, F.; Walton, R. I. Crystallisation Kinetics of Metal Organic Frameworks From in Situ Time-Resolved X-Ray Diffraction. *Powder Diffraction*. **2013**, *28* (S2), S256–S275. <https://doi.org/10.1017/S0885715613000997>.
- (34) Koslowski, T.; Ludwig, U. Retardation of Gypsum Plasters with Citric Acid: Mechanism and Properties. In *The Chemistry and Technology of Gypsum*; ASTM International: 100 Barr Harbor Drive, PO Box C700, West Conshohocken, PA 19428-2959, 1984; pp 97–104. <https://doi.org/10.1520/STP30274S>.
- (35) Rejab, L. T.; Al-Jubori, S. Examination of the Particle's Shape, Size and Distribution of the Commercial Dental Gypsum Products. *Al-Rafidain Dent. J.* **2003**, *3* (2), 103–107. <https://doi.org/10.33899/rden.2003.165764>.
- (36) Abu Zeitoun, E.; Pritzel, C.; Sakalli, Y.; Trettin, R. The Mechanism of the First Hydration-Dehydration Cycle of Pure  $\alpha$  - and  $\beta$  -CaSO<sub>4</sub> •0.5H<sub>2</sub>O. *Adv. Mater. Sci. Eng.* **2020**, *2020*, 1–11. <https://doi.org/10.1155/2020/1732621>.
- (37) De Bruijn, T. J. W.; De Jong, W. A.; Van Den Berg, P. J. Kinetic Parameters in Avrami-Erofeev Type Reactions from Isothermal and Non-Isothermal Experiments. *Thermochim. Acta* **1981**, *45* (3), 315–325. [https://doi.org/10.1016/0040-6031\(81\)85091-5](https://doi.org/10.1016/0040-6031(81)85091-5).
- (38) Salas, G.; Costo, R.; Morales, M. del P. Synthesis of Inorganic Nanoparticles. *Nanobiotechnology Inorg. nanoparticles vs Org. nanoparticles* **2012**, *4*, 35–79. <https://doi.org/10.1016/B978-0-12-415769-9.00002-9>.
- (39) Lide, D. Aqueous Solubility of Inorganic Compounds at Various Temperatures. In *CRC Handbook of Chemistry and Physics*; 2005; pp 112–117.
- (40) Hamdona, S. K.; Hamza, S. M. Influence of Some Phosphates and Polyphosphate on the Precipitation of Calcium Sulfate Dihydrate in Sodium Chloride Solutions. *J. Taibah Univ. Sci.* **2009**, *2* (1), 44–51. [https://doi.org/10.1016/s1658-3655\(12\)60006-5](https://doi.org/10.1016/s1658-3655(12)60006-5).
- (41) Sakae, T.; Nagata, H.; Sudo, T. The Crystal Structure of Synthetic Calcium Phosphate-Sulfate Hydrate and Its Relation to Brushite and Gypsum. *Am. Mineral.* **1978**, *63*, 520–527.
- (42) Comodi, P.; Nazzareni, S.; Zanazzi, P. F.; Speziale, S. High-Pressure Behavior of Gypsum: A Single-Crystal X-Ray Study. *Am. Mineral.* **2008**, *93* (10), 1530–1537.

<https://doi.org/10.2138/am.2008.2917>.

- (43) Cravillon, J.; Schröder, C. A.; Bux, H.; Rothkirch, A.; Caro, J.; Wiebcke, M. Formate Modulated Solvothermal Synthesis of ZIF-8 Investigated Using Time-Resolved in Situ X-Ray Diffraction and Scanning Electron Microscopy. *CrystEngComm* **2012**, *14* (2), 492–498.  
<https://doi.org/10.1039/C1CE06002C>.
- (44) Kashchiev, D. *Nucleation. Basic Theory with Applications*, 1st ed.; ButterHeinem ST: Oxford, 2000.
- (45) Cubillas, P.; Anderson, M. W. Synthesis Mechanism: Crystal Growth and Nucleation. In *Zeolites and Catalysis: Synthesis, Reactions and Applications*; Čejka, J., Corma, A., Zones, S., Eds.; Wiley-VCH Verlag GmbH & Co. KGaA: Weinheim, Germany, 2010; Vol. 1, pp 1–55.
- (46) Qu, J. D.; Peng, J. H.; Li, B. Z. Effect of Citric Acid on the Crystal Morphology of Gypsum and Its Action Mechanism. *Adv. Mater. Res.* **2011**, *250–253*, 321–326.  
<https://doi.org/10.4028/www.scientific.net/AMR.250-253.321>.